Thermodynamics of lattice QCD with two light quarks on a $16^3 \times 8$ lattice

Steven Gottlieb and A. Krasnitz
Department of Physics, Indiana University, Bloomington, Indiana 47405

U. M. Heller and A. D. Kennedy
Supercomputer Computations Research Institute, The Florida State University, Tallahassee, Florida 32306-4052

J. B. Kogut
Department of Physics, University of Illinois, 1110 West Green Street, Urbana, Illinois 61801

R. L. Renken
Department of Physics, University of Central Florida, Orlando, Florida 32816

D. K. Sinclair
HEP Division, Argonne National Laboratory, 9700 South Cass Avenue, Argonne, Illinois 60439

R. L. Sugar
Department of Physics, University of California, Santa Barbara, California 93106

D. Toussaint
Department of Physics, University of Arizona, Tucson, Arizona 85721

K. C. Wang
School of Physics, University of New South Wales, PO Box 1, Kensington, NSW 2203, Australia
(Received 14 September 1992)

We have carried out a numerical study of the high-temperature behavior of lattice QCD with two flavors of staggered quarks. Our simulations were performed on $16^3 \times 8$ lattices with a quark mass $m_q = 0.0125$, in units of the inverse lattice spacing. By monitoring the Wilson-Polyakov line, the chiral order parameter $\langle \bar{\psi}\psi \rangle$, and the average plaquette, we have determined that a crossover between the low-temperature state of ordinary hadronic matter and the high-temperature quark-gluon plasma occurs at a gauge coupling of $6/g^2 = 5.54(2)$. Thermodynamic quantities do not show a large jump, although the equilibration time becomes quite long in the vicinity of the crossover. We have measured the entropy densities in the neighborhood of the crossover and further into the plasma phase. Measurements of the hadronic screening lengths and the Debye screening lengths were made which cast light on the differences between the two regimes. Finally, we measured the topological susceptibilities to further explore the chiral properties of QCD.

PACS number(s): 12.38.Gc, 11.15.Ha

I. INTRODUCTION

An understanding of quantum chromodynamics at finite temperatures is one of the major objectives of lattice gauge theory. It is expected that hadronic matter undergoes a rapid crossover or phase transition from its ordinary low-temperature state to a high-temperature state consisting of a plasma of quarks and gluons. The nature of this crossover and of the high-temperature state are important for an understanding of the dynamics of QCD, particularly with regard to chiral symmetry and confinement. Nuclear physicists hope to observe the high-temperature state in heavy-ion collisions planned for new accelerators such as the BNL Relativistic Heavy Ion Collider. A detailed knowledge of the properties of this state could provide experimentalists with guides to signatures for identifying it. Immediately after the big bang, the Universe was presumably in the high-temperature state, and therefore must have passed through the crossover region as it cooled. Thus, a knowledge of the properties of the quark-gluon plasma and the crossover are necessary in order to understand the evolution of the early universe.

We are carrying out simulations of lattice QCD with two flavors of staggered quarks on $16^3 \times 8$ lattices using the connection machine (CM-2) at the Pittsburgh Supercomputer Center. In this paper, we present results for the quark mass $m_q = 0.0125$ in lattice units [1]. We are in the process of extending this work to $m_q = 0.006\,25$. Although both of these masses are larger than the physical values for the u and d quarks, it is hoped that they are small enough to allow extrapolation to the chiral limit. We are using the hybrid molecular dynamics algorithm with noisy fermions [2] which allows us to tune the number of flavors to two. We have performed simulations in the neighborhood of the crossover in order to study the

nature of the transition. We have also carried out studies of the quark-gluon plasma at temperatures well above the crossover. We have not found evidence for a first-order transition. This result is consistent with previous studies on lattices with four and six time slices [3], and with chiral spin models [4] which indicate a first-order transition for three and four flavors of zero-mass quarks, but a second-order transition for two flavors of zero-mass quarks. By combining our results with recent spectrum calculations we have made an improved estimate of the crossover temperature in MeV.

In addition to measuring the Wilson-Polyakov line, the chiral order parameter $\langle \bar{\psi}\psi \rangle$, and the average plaquette, we have studied the entropy density of the system and the partial entropy densities, and have measured the topological susceptibility of the system using the cooling method [5]. We have studied the hadronic screening lengths for those hadrons which are produced by sources local in the quark field, as well as the screening length for the quark itself. For these studies, we have used wall sources [6] to enhance the signal. Our results are consistent with earlier studies of screening lengths at larger lattice spacings [7–9] and are similar to those for four light quark flavors measured on the same size lattice [10]. For temperatures below the crossover, the screening masses are similar to the zero-temperature hadron masses. For temperatures above the crossover, the screening masses become parity doubled, suggesting the restoration of chiral symmetry. The ρ-a_1 and N-N' screening masses appear to approach the values $2\pi T$ and $3\pi T$, respectively, in the high-temperature regime, which is consistent with the suggestion of Irbäck [10] that these are unbound multiquark states. The screening lengths are also consistent with the scenario recently suggested by Gocksch [11]. However, we know from the study of the spatial structure of screening propagators that there are strong correlations among the quarks in the high-temperature state [12], and that a nonzero string tension can be associated with purely spatial Wilson loops (see Sec. II). Finally, we have studied the correlations of Wilson-Polyakov lines, oriented both in the time direction where these correlations are related to the potential for static quarks and exhibit Debye screening in the plasma phase, and in the spatial directions, where they measure properties of a three-dimensional Yang-Mills-Higgs system with quarks, which describes the high-temperature behavior of QCD. For these studies we have used the "fuzzy" Wilson-Polyakov lines of Teper [13] to improve the signal-to-noise ratio.

In Sec. II, we describe our runs and present results for the simpler order parameters, Wilson-Polyakov line correlations, and topological susceptibility. In Sec. III, we discuss our results for the hadron screening lengths, and in Sec. IV, we present our conclusions. Finally, in an appendix we give a brief description of some of the order parameters and the methods used to calculate and analyze them.

II. THE SIMULATIONS

We have carried out simulations with two degenerate flavors of staggered quarks with a mass $am_q = 0.0125$ on $16^3 \times 8$ lattices. We have used the hybrid molecular-dynamics algorithm which is described in detail in Ref. [2]. These simulations use code developed by the HEMCGC Collaboration [14]. The algorithm includes a numerical integration of the nonlinear equations of motion for the gauge fields. This integration was performed with a time step $dt = 0.01$ in the HEMCGC normalization [15]. One thousand molecular-dynamics time units were collected at gauge couplings $6/g^2 = 5.45$, 5.60, 6.0, and 7.0, two thousand at $6/g^2 = 5.5$ and 5.525, and 750 at $6/g^2 = 5.575$. Two runs of 1500 time units were made at $6/g^2 = 5.55$, one beginning from a lattice in the high-temperature state, and one from a lattice in the low-temperature state. These runs appeared to be long enough to allow the system to equilibrate at each value of $6/g^2$, and to enable us to collect adequate statistics for the simple order parameters, after equilibration. In addition, configurations were stored every 5 time units at $6/g^2 = 5.45$ and 5.5, every 10 time units at $6/g^2 = 5.525$, 5.55, 5.575, and 5.6, and every 50 time units at $6/g^2 = 6.0$ and 7.0, for further analysis.

Table I shows the values of the Wilson-Polyakov lines and $\langle \bar{\psi}\psi \rangle$ as functions of $6/g^2$, along with the length of the runs and the number of time units discarded for equilibration. These results are plotted in Fig. 1. Here, in Fig. 1 and Table I, the results at $6/g^2 = 5.55$ are from the run begun in the high-temperature state. They suggest that the restoration of chiral symmetry occurs for $5.525 \lesssim 6/g^2 \lesssim 5.55$. In Fig. 2, we plot the time histories of the Wilson-Polyakov line and the chiral order parameter $\langle \bar{\psi}\psi \rangle$ for couplings in the range $5.45 \leq 6/g^2 \leq 5.575$. In Fig. 3, we show the Wilson-Polyakov line and $\langle \bar{\psi}\psi \rangle$ for the two runs at $6/g^2 = 5.55$ with starts in the high- and low-temperature states. These time histories indicate that the equilibration time in the vicinity of the crossover is quite long, but there is no evidence of the type of metastability found close to a first-order phase transition. Our results are consistent with a second-order transition at zero quark mass as predicted by the chiral spin model analysis [4], and a rapid crossover rather than a true phase transition for small quark mass.

To help the reader draw his own conclusions from this time evolution data, we give here a brief description of the starting points for each of our runs. The high-temperature run at $\beta = 5.55$ was started from an ordered ($\beta = \infty$) configuration. The $\beta = 5.5$ run was started from an early (unequilibrated) configuration at $\beta = 5.55$ (hot),

TABLE I. Wilson-Polyakov line and $\langle \bar{\psi}\psi \rangle$ as functions of $6/g^2$ on a $16^3 \times 8$ lattice with $m_q = 0.0125$. Errors are from binning with extrapolation.

$6/g^2$	Wilson line	$\langle \bar{\psi}\psi \rangle$	Time (discarded)
5.450	0.0101(39)	0.2546(51)	1000(200)
5.500	0.0306(45)	0.1805(30)	2000(300)
5.525	0.0356(34)	0.1570(25)	2000(300)
5.550	0.0702(17)	0.1146(20)	1500(200)
5.575	0.0817(21)	0.1029(30)	750(250)
5.600	0.0812(48)	0.0974(21)	1000(200)
6.000	0.2089(33)	0.05840(8)	1000(100)
7.000	0.4646(36)	0.04172(2)	1000(100)

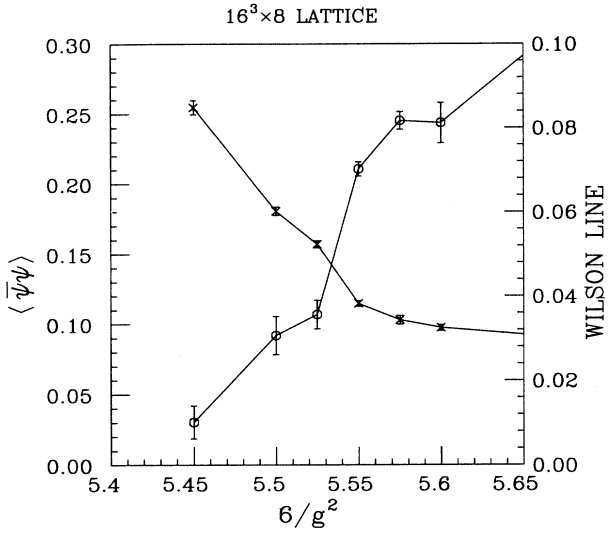

FIG. 1. The Wilson-Polyakov line and $\langle\bar{\psi}\psi\rangle$ as functions of $6/g^2$.

while those at $\beta=5.6$ and 5.525 were started from better equilibrated configurations from this $\beta=5.55$ run. A partially equilibrated configuration at $\beta=5.5$ was used to start the $\beta=5.45$ run, while the low-temperature run at $\beta=5.55$ started from the final configuration of the $\beta=5.5$ simulation. A $\beta=5.55$ (cold) configuration equilibrated for 1000 time units was used to start the $\beta=5.575$ run. Finally, the $\beta=7.0$ run used an ordered start, and an equilibrated configuration at this β was used to start the $\beta=6.0$ run.

By combining thermodynamics results with zero-temperature spectrum calculations at the same lattice spacing and quark mass, one can estimate the crossover temperature T_c in MeV from the relation [16]

$$T_c=\frac{m_e}{mN_t}\ . \tag{2.1}$$

The quantity m_e in the numerator of Eq. (2.1) is the mass of a hadron taken from experiment, while the quantity m in the denominator is the mass of the same hadron in lattice units measured in a spectrum calculation. N_t is the

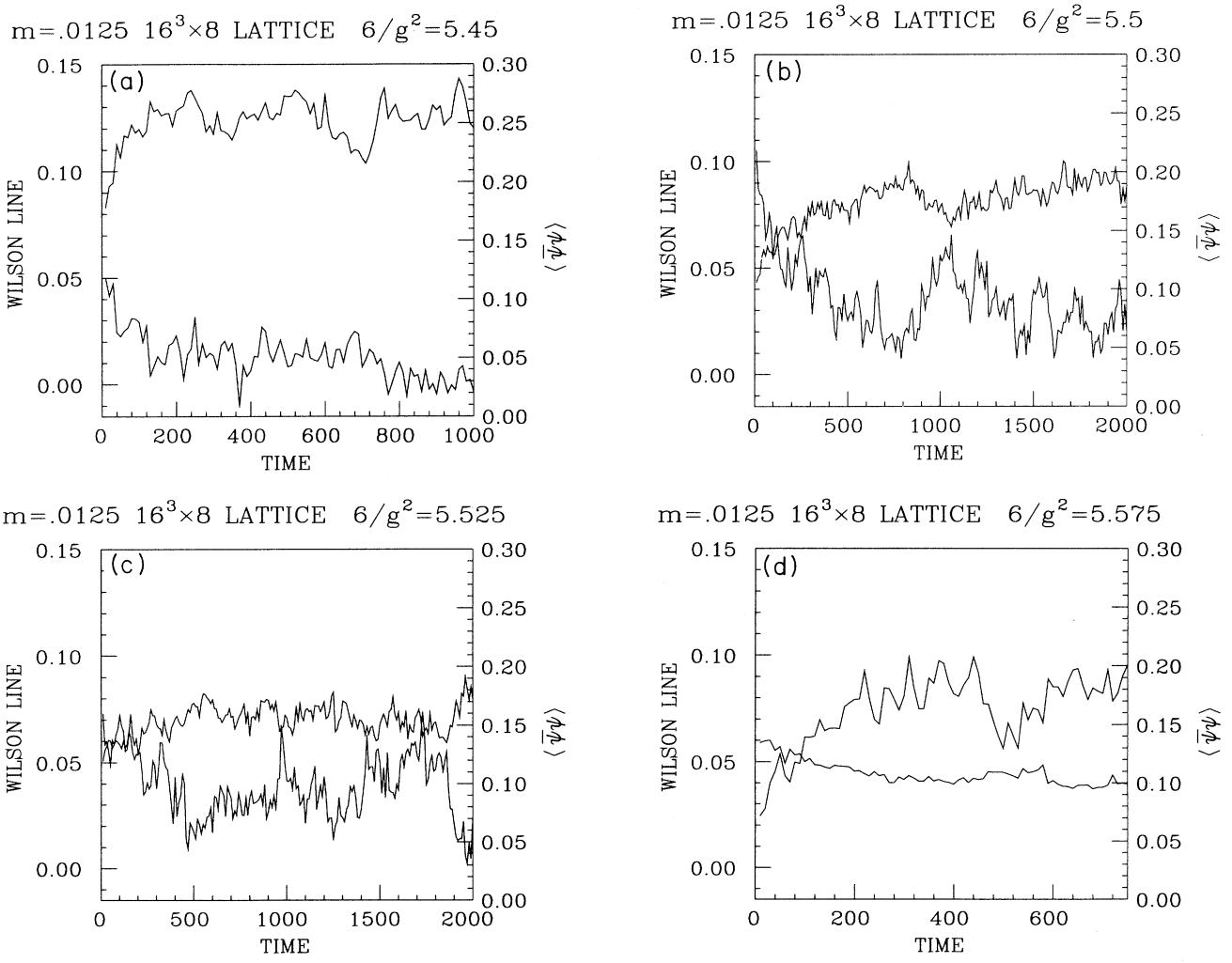

FIG. 2. Time histories of the Wilson-Polyakov line and $\langle\bar{\psi}\psi\rangle$ for (a) $6/g^2=5.45$, (b) $6/g^2=5.5$, (c) $6/g^2=5.525$, and (d) $6/g^2=5.575$. $\langle\bar{\psi}\psi\rangle$ is the upper curve in (a), (b), and (c), and the lower curve in (d).

number of time slices in the thermodynamics calculation, eight in the present case. Although we have not carried out a spectrum calculation precisely at the crossover coupling, calculations have been made with values of $6/g^2$ and m_q close enough to the values used here to allow an extrapolation to $6/g^2=5.54$ [15,17,30]. Specifically, we have spectrum studies at $6/g^2=5.415$ and $m_q=0.0125$, at $6/g^2=5.6$ with $m_q=0.01$ and 0.025, and $6/g^2=5.7$ with $m_q=0.015$, 0.020, and 0.025. The ρ mass at $m_q=0.0125$ was estimated by linear interpolation at $6/g^2=5.6$ and by linear extrapolation at 5.7. We note that although there is a calculation at the weakest coupling for quark mass 0.01, the four ρ masses do not fall on a straight line. The lightest mass is the one most likely to be affected by finite size effects. We have, therefore, chosen to extrapolate using the three higher masses. With the ρ mass in hand for three values of the coupling, we estimate its value at intermediate values of the coupling by a fit of the form

$$\ln(m_\rho)=a+b(6/g^2)+c(6/g^2)^2 .$$

Using the ρ meson mass to set the energy scale, we find $T_c=155\pm9$ MeV. An error of 9 MeV comes from our uncertainty in the value of $6/g^2$ at the high-temperature crossover, a quantity which is not even precisely defined if there is no phase transition. This quoted error is the statistical error only; the systematic effects are much larger. For example, using the nucleon to set the scale gives a result lower by about 15%. In addition, there is an uncertainty of around 6 MeV coming from the interpolation necessary to estimate the hadron masses. We estimate this error from the difference in the hadron masses interpolated using the form above and those using a linear interpolation.

In Fig. 4, we plot T_c for two flavors of staggered quarks as a function of N_t, again using the ρ mass to set the energy scale. The results from simulations with dynamical quarks are denoted by fancy crosses, and those from the quenched approximation are denoted by squares. The dynamical quark points for $N_t=4$ and 6 are from Refs. [16] and [18], respectively. The quenched points were obtained by combining the thermodynamics studies of [19] with quenched spectrum studies of a number of groups [20]. In some cases, more than one quenched point is shown because more than one quenched spectrum calculation was available. All thermodynamics and spectrum calculations, except those from the present study, were extrapolated to $m_q=0$. Although the dynamical quark calculations are not at small enough lattice spacings to be in the perturbative scaling regime, the fact that T_c is quite insensitive to N_t for both the dynamical and quenched studies provides reason to believe that these results are significant. At the very least, it is clear that the value of T_c for full QCD is considerably below that for the quenched approximation, as one would expect.

In Table II we give the energy plus pressure, or entro-

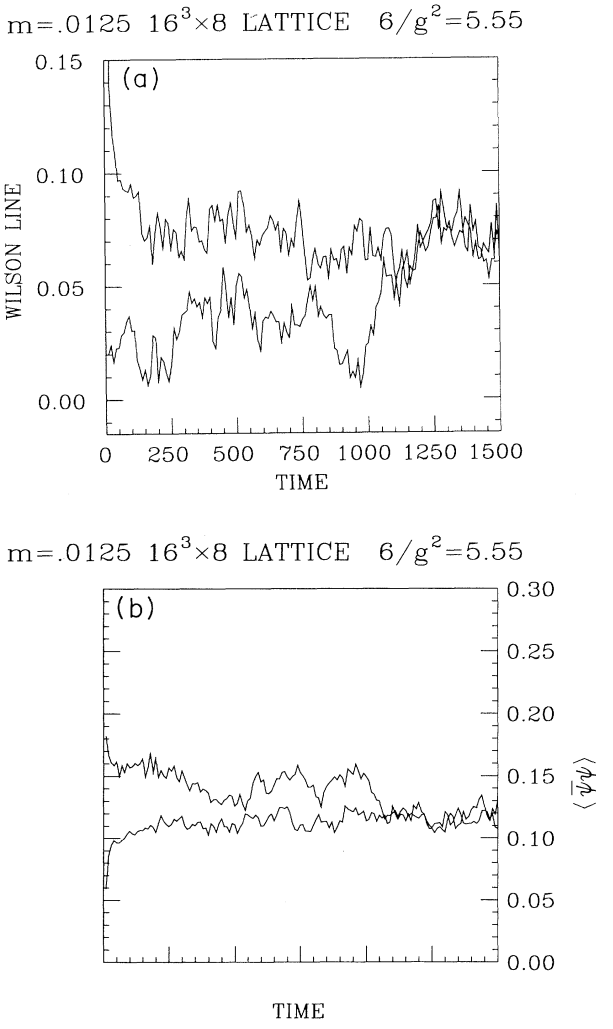

FIG. 3. Time histories of the Wilson-Polyakov line for $6/g^2=5.55$. The upper curve is from a hot start, the lower from a cold start. (b) Time histories of $\langle\bar{\psi}\psi\rangle$ for $6/g^2=5.55$. The lower curve is from a hot start, the upper from a cold start.

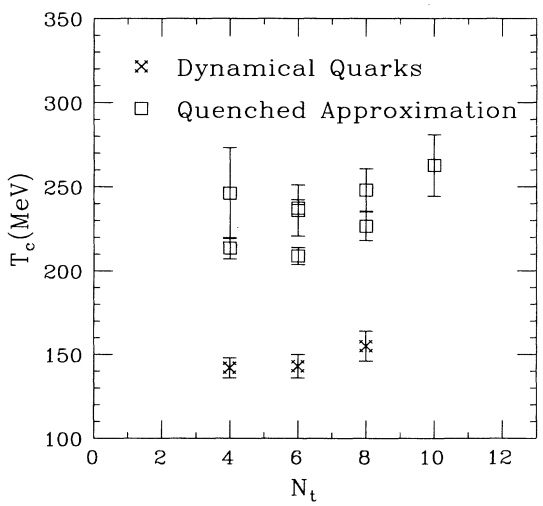

FIG. 4. The transition temperature T_c as a function of N_t in laboratory units.

TABLE II. Partial entropy densities for the gluons (s_g) and u and d quarks ($s_{u,d}$), including the one-loop [$O(g^2)$] corrections, but not the finite-volume corrections.

$6/g^2$	s_g/T^3	$s_{u,d}/T^3$
5.450	−0.7(4.0)	0.7(1.0)
5.500	1.8(2.3)	2.7(7)
5.525	3.6(2.2)	2.5(6)
5.550	5.0(3.2)	6.3(6)
5.575	10.6(5.1)	7.6(9)
5.600	11.0(3.8)	5.7(7)
6.000	9.9(2.9)	8.3(6)
7.000	8.5(3.1)	9.1(5)

TABLE III. Partial entropy densities for the gluons (s_g) and u and d quarks ($s_{u,d}$), at tree level and average plaquettes. $P=1-\frac{1}{6}(P_{ss}+P_{st})$.

$6/g^2$	s_g^0/T^3	$s_{u,d}^0/T^3$	P
5.450	−0.8(4.9)	0.8(1.4)	0.458 31(15)
5.500	2.2(2.9)	3.5(9)	0.449 20(9)
5.525	4.4(2.2)	3.3(8)	0.445 42(5)
5.550	6.2(4.0)	8.2(7)	0.441 16(5)
5.575	13.0(6.2)	9.9(1.1)	0.437 59(11)
5.600	13.4(4.7)	7.3(9)	0.434 44(7)
6.000	11.9(3.4)	10.5(7)	0.405 19(4)
7.000	10.0(3.6)	11.1(6)	0.322 42(3)

py, including the one-loop perturbative corrections [21,22]. In an attempt to remove some of the effects of finite spatial volume, we have divided each of the partial entropies by the ratio of its free field value on a $16^3\times 8$ lattice to its continuum value in an infinite spatial volume at $T=\frac{1}{8}$ (lattice units) [23]. These ratios are 0.991 36 for the gluons and 1.597 18 for the u and d quarks. These values are plotted in Fig. 5 and compared with the Stefan-Boltzmann constant. We see that the gluon and u,d values show a rapid increase from near zero as one passes through the transition. The gluon entropy density appears to overshoot the Stefan-Boltzmann value ($32\pi^2/45$) and to approach it from above for large $6/g^2$. The u and d quark entropy density increases somewhat more slowly with increasing $6/g^2$ than on smaller lattices [this is somewhat deceptive, since some of the published data on smaller lattices does not include the $O(g^2)$ corrections which decreased even our $6/g^2=7.0$ data by 18%], and will presumably approach the Stefan-Boltzmann value ($7\pi^2 n_f/15$) from below as $6/g^2\to\infty$. In Fig. 5(b) we have included the entropy of a heavy ($m_s=0.25$) quark calculated in the gauge fields generated with two light quarks in the action. Although we have labeled it "s" since its mass is 20 times that of our u and d quarks, because our u and d quarks are unphysically heavy, its mass is large enough that it does not really see the transition. In Table III we present the zeroth-order entropies [(A1) and (A2) without the one-loop corrections] together with the average plaquette values, so that when the $T=0$ plaquettes become available the reader can extract the energy density and pressure, and for the benefit of anyone with a nonperturbative estimate of the coefficients.

We measured the topological charge by the cooling method outlined in the Appendix (subsection 2). In Table IV, we list values for the topological susceptibility χ determined by the normal cooling method, using 25 cooling sweeps, and by the underrelaxed method described in the Appendix, subsection 2 using $\lambda=0.2$ for 25 sweeps followed by 25 sweeps of normal cooling. The results of the two methods are clearly consistent. The two results given for each method labeled EO and OE are the values obtained when we chose to start with the even and odd sublattice respectively for the cooling. The final column labeled "theory" gives the value predicted by Eq. (A3) [24] using the values of $\langle\bar{\psi}\psi\rangle$ obtained on a $12^3\times 8$ lattice at $m_q=0.025$ and $m_q=0.0125$ [25] linearly extrapolated to $m_q=0$. For $6/g^2$ in the low-temperature (hadronic) state, the agreement is excellent. For the high-temperature (plasma) state, the extrapolated values of

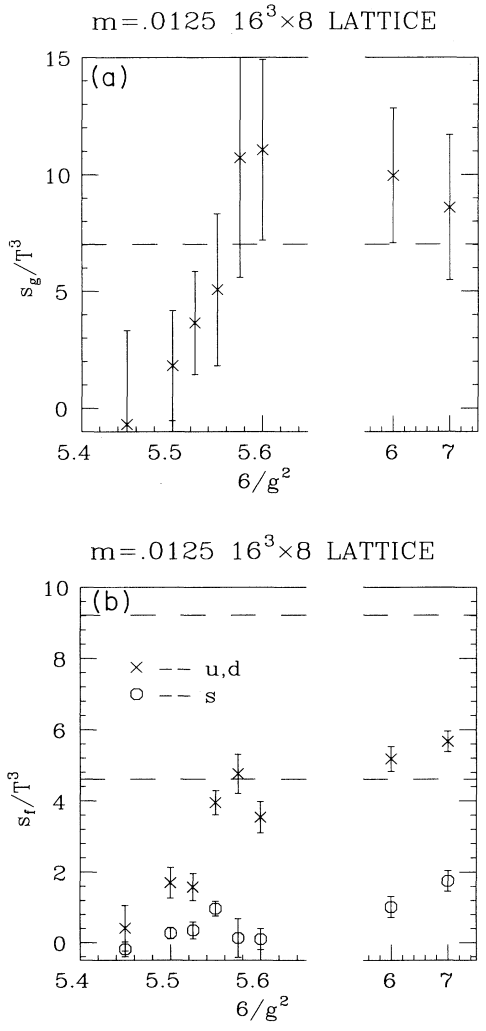

FIG. 5. Entropy densities as a function of $6/g^2$ for (a) the gluons, and (b) the quarks. The dashed lines are the Stefan-Boltzmann limit. In (b) the upper dashed line is that for the u and d quarks, the lower for the "s" quark.

TABLE IV. Topological susceptibility χ as a function of temperature. The four columns of measurements use the methods described in the text. The column labeled theory gives results obtained from the anomalous Ward identity using the values obtained for $\langle\bar{\psi}\psi\rangle$ on a $12^3\times 8$ lattice [25].

	$\chi\times 10^5$				
	Normal cooling		Underrelaxed		
$6/g^2$	EO	OE	EO	OE	Theory
5.450	24.6(5.1)	25.6(5.1)	24.1(5.2)	23.1(4.5)	25.6(2.0)
5.500	13.9(1.5)	13.8(1.7)	13.6(1.5)	13.2(1.6)	12.8(2.5)
5.525	10.8(1.8)	11.3(1.6)	10.4(1.7)	10.6(1.7)	
5.550	3.4(6)	3.0(6)	2.9(5)	2.9(5)	−0.9(2.0)
5.575	1.8(5)	2.0(6)	1.5(5)	1.7(5)	
5.600	2.3(6)	2.3(7)	2.2(6)	2.2(6)	−1.6(1.4)
5.650					0.6(9)
5.700					0.1(2.0)
6.000	0	0	0	0	
7.000	0	0	0	0	

$\langle\bar{\psi}\psi\rangle$ are consistent with zero, as they should be. The values of χ are small but nonzero (except for $6/g^2=6.0$ and 7.0). This is understandable since (A3) only yields the term linear in m_q, whereas theory predicts that $\chi\propto m_q^2$ in this phase [Eq. (A3)].

We have studied the correlations between "fuzzy" temporal Wilson lines. We have measured correlations in the z direction for lines with zero x and y components of momentum. (See Appendix, subsection 3 for details.) We have considered blocking levels from 0 (unblocked) to 3 (blocked link length 8), and found that, as is the zero-temperature case, blocking greatly improved the signal-to-noise ratio by enhancing the overlap of the line operator with the lowest-lying excitation, enabling us to estimate the mass using correlations at shorter distances. This is exhibited for a typical subtracted correlation function in Fig. 6. Hence, from now on, we will deal exclusively with blocking level 3 propagators.

Since, in contrast with the case of pure Yang-Mills gauge theories, the Wilson-Polyakov line has a nonzero vacuum expectation value in both phases, we expect screening for all values of the gauge coupling. Such screening can be small, as it appears to be at zero temperature. If so, an exponential falloff in the subtracted propagator at intermediate distances might still measure the string tension rather than the eventual potential screening at large distances. To decide what is the correct interpretation, one needs to look also at the unsubtracted correlation functions. If, as is the case at zero temperature, the subtracted and unsubtracted correlation functions are very similar, one is probably in a region where the string tension drives the exponential falloff [26]. If the unsubtracted propagator rapidly flattens off to a nonzero value determined by the magnitude squared of the expectation value of the Wilson-Polyakov line, then the exponential falloff of the subtracted propagator yields the screening length [27].

In Fig. 7, we have plotted the unsubtracted Wilson-Polyakov line correlations, normalized to one at $Z=0$ as a function of the separation Z. In each case, we do observe flattening at large Z. It is interesting to note the rapid change in behavior of these propagators between $6/g^2=5.525$ and 5.55 which marks the crossover. For $6/g^2\geq 5.55$ one would clearly interpret an exponential falloff in the subtracted propagator as screening. For $6/g^2=5.45$ an exponential falloff at short distances might be associated with a linear potential which is screened at longer distances. At intermediate values of $6/g^2$ (5.5 and 5.525) screening is very apparent at all Z, but the screening lengths we have obtained for these values of $6/g^2$ should not be trusted, since some of the falloff is still probably due to the string tension.

We have studied the large distance behavior of the subtracted correlation functions in the manner described in the Appendix, subsection 3. The screening length was determined by calculating the effective mass from Eq. (A24). In order to obtain a reliable result, one must find a plateau in $\mu(Z)$ before the signal is obscured by noise.

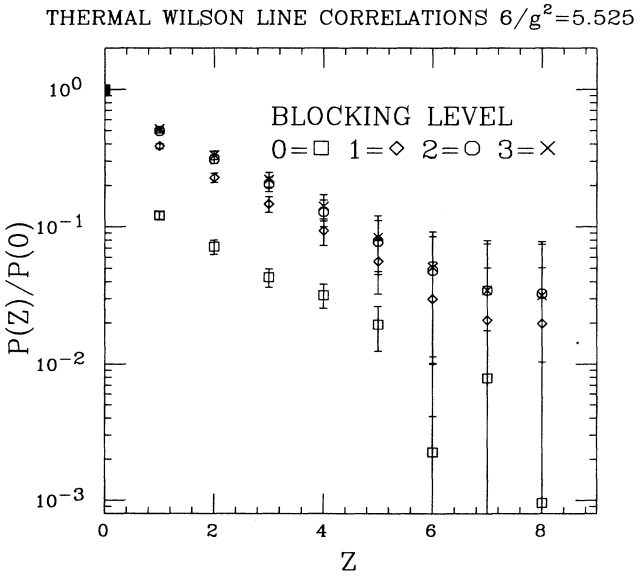

FIG. 6. Subtracted thermal Wilson-Polyakov line correlation functions as a function of separation Z at $6/g^2=5.525$ for blocking levels 0–3.

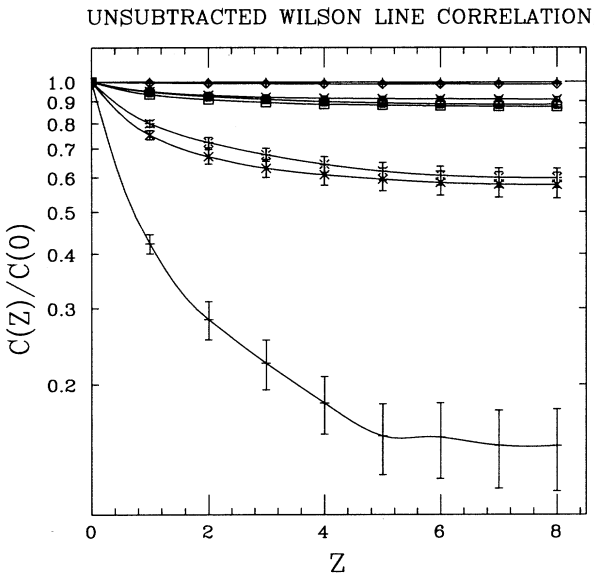

FIG. 7. Unsubtracted Wilson-Polyakov line correlations as a function of Z for various $6/g^2$ values. The curves, from the lowest lying to the highest correspond to $6/g^2=5.45$, 5.5, 5.525, 5.55, 5.6, 5.575, 6.0, and 7.0.

Our results are tabulated in Table V. The data shows some evidence for a plateau, at least in the high-temperature phase, which is where we argued that the simple screening interpretation was clear. Using the criterion that useful data should have errors $\lesssim 15\%$ we see that we are limited to using $\mu(Z \lesssim 3)$. Fortunately, our data suggest that the plateaus are reached by $Z=2$, so that we can estimate the screening mass from $\mu(2)$ or $\mu(3)$. The quantity of interest is μ/T, where here $T=1/8a$. Using $\mu(2)$ as our estimate of μ, then in the quark-gluon plasma phase, this quantity takes the values 5.3(5) at $6/g^2=5.55$, 3.6(4) at $6/g^2=5.6$, 4.0(6) at $6/g^2=6.0$, and 4.5(4) at $6/g^2=7.0$. These values are in good agreement with the $N_t=4$ results [28], but a little larger than those reported for pure SU(3) Yang-Mills theory, possibly due to the extra screening afforded by the quarks [27].

In addition to considering Wilson-Polyakov lines oriented in the time direction, we have also considered

TABLE V. Effective masses $[\mu(Z)]$ from subtracted blocked temporal Wilson-Polyakov line correlation functions (blocking level 3).

	Temporal Wilson-Polyakov line effective mass			
$6/g^2$	$Z=0-1$	$Z=1-2$	$Z=2-3$	$Z=3-4$
5.450	1.09(7)	0.63(8)	0.42(11)	0.49(22)
5.500	0.77(5)	0.49(6)	0.38(5)	0.30(8)
5.525	0.66(4)	0.45(5)	0.41(7)	0.47(12)
5.550	0.83(4)	0.66(6)	0.71(12)	1.13(47)
5.575	0.83(8)	0.68(12)	0.69(23)	0.57(30)
5.600	0.63(5)	0.45(5)	0.45(9)	0.55(25)
6.000	0.63(5)	0.49(7)	0.48(10)	0.57(22)
7.000	0.61(3)	0.56(5)	0.61(11)	0.71(25)

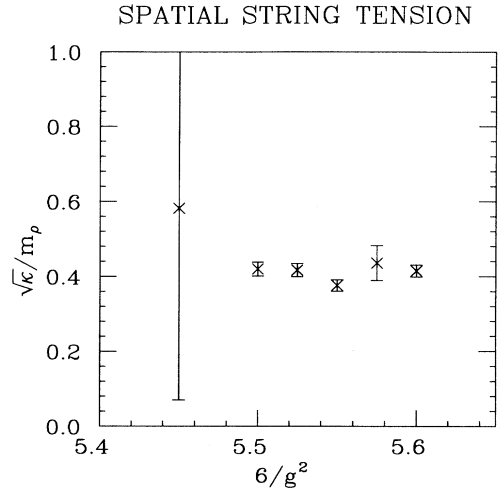

FIG. 8. Graph showing the $6/g^2$ dependence of the string tension κ calculated from spatial Wilson-Polyakov line correlations.

those oriented in the x and y spatial directions. Here, previous studies have indicated that the correlation functions should obey an area law, i.e., should be confining, for all values of $6/g^2$ [29]. Since these spatial lines have small but nonzero vacuum expectation values coming from the limited spatial extent of the lattice, we compared the subtracted and unsubtracted correlation functions. Again, blocking improves the signal-to-noise ratio, so we will concentrate only on the level 3 propagators. For all values of $6/g^2$ except 6.0 and 7.0, there are no significant differences between the subtracted and unsubtracted propagators indicating the "deconfinement in the spatial direction" is relatively unimportant in this coupling domain. For $6/g^2=6.0$, the difference between subtracted and unsubtracted propagators is still small enough that the difference between the effective mass estimated from the subtracted and unsubtracted propagators is still $\lesssim 10\%$. For $6/g^2=7.0$, the effect is larger, resulting in a difference of $\approx 25\%$ in the effective mass. At $6/g^2=7.0$ the lattice spacing is small enough that even an $N_t=16$ lattice would be in the deconfined phase, so we should not expect to see "spatial confinement." For $6/g^2=6.0$ we might be close to the deconfinement coupling for an $N_t=16$ lattice. The effective mass values from the subtracted propagators are presented in Table VI. Unfortunately, at $6/g^2=5.45$ the statistics are too

TABLE VI. Effective masses from subtracted blocked spatial Wilson-Polyakov line correlation functions (blocking level 3).

	Spatial Wilson-Polyakov line effective mass			
$6/g^2$	$Z=0-1$	$Z=1-2$	$Z=2-3$	$Z=3-4$
5.450	2.90(9)	3.47(6.11)		
5.500	2.13(5)	1.37(12)	1.66(73)	
5.525	1.92(5)	1.18(10)	1.12(29)	0.25(30)
5.550	1.49(3)	0.84(7)	0.83(11)	0.33(14)
5.575	1.41(9)	0.99(21)	1.18(59)	
5.600	1.32(6)	0.79(6)	0.78(13)	0.98(24)
6.000	0.55(3)	0.44(3)	0.45(6)	0.47(13)
7.000	0.20(3)	0.18(3)	0.17(3)	0.17(3)

poor to extract a reliable string tension to compare with zero-temperature results. In Fig. 8, we plot the quantity $\sqrt{\kappa}/m_\rho$ where κ is the string tension calculated as the effective mass calculated between $Z=1$ and $Z=2$ (which appears to herald the onset of the plateau) divided by $N_s=16$. The ρ mass is estimated from interpolation among spectrum calculations at $6/g^2=5.415$, 5.6, and 5.7 [15,17,30].

III. HADRONIC SCREENING LENGTHS

We have made measurements of the propagators in the spatial direction of color singlet hadronic sources, or the "hadronic screening lengths" [7–9,18], using the wall sources defined in the Appendix, subsection 4 to enhance the signal. We are limited in this study by the fact that we worked on lattices with a maximum spatial dimension of only twice the Euclidean time dimension, so that we could measure screening propagators only for distance less than or equal to $1/T$. Therefore, there is some doubt as to whether we have really found the asymptotic mass in these propagators. In many cases, we were unable to find fits with satisfactory χ^2, and there are not visible "plateaus" in the effective mass versus distance.

Figures 9(a) and 9(b) show our best estimates of the screening masses for the scalar- and vector-meson channels, and Fig. 9(c) shows the baryon channel. In all cases, we see parity doubling for $6/g^2 \gtrsim 5.55$. For the vector channels we see the ρ and a_1 become degenerate, while the other pointlike ρ, the ρ_2, becomes degenerate with the b_1. Both the ρ_2 and b_1 signals become very difficult to extract as $6/g^2$ grows.

Within the limitations of our small lattice, we find the expected pattern of parity doubling at high temperatures, characteristic of chiral symmetry restoration. Moreover, as has been emphasized previously in Refs. [10,11], the screening masses of the vector mesons are very close to twice the Matsubara frequency. The screening masses of the baryons are larger than three times the Matsubara frequency. We note in passing that, if the baryonic states were indeed states of 3 free quarks, the screening masses calculated as if the baryons were one-particle states would be expected to lie above $3\pi T$. This is due to the finite spatial extent of the lattice; in particular, to the fact that with dynamical quarks, as in free field theory, two of the quarks can propagate forward (in z) from the source

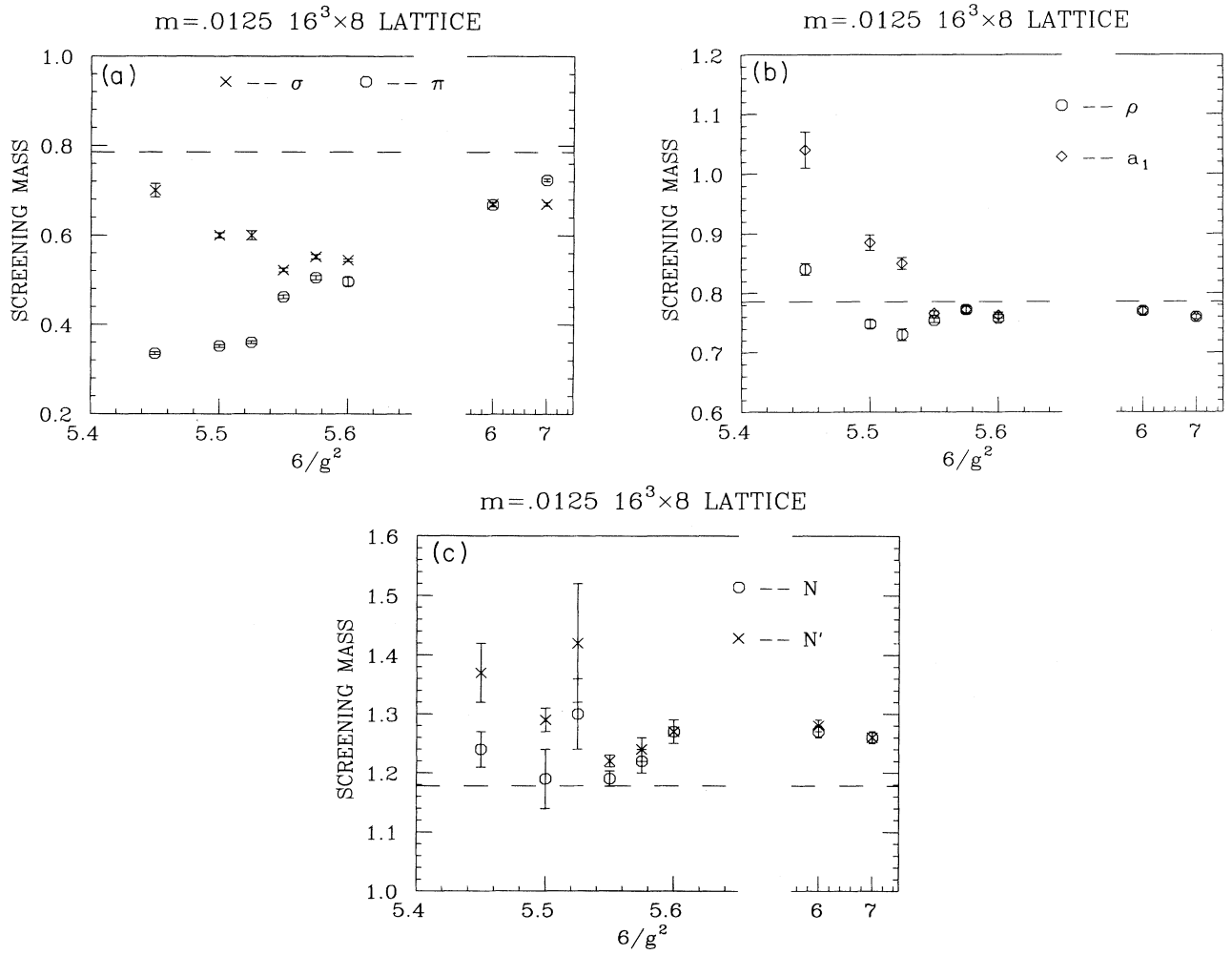

FIG. 9. Hadron screening lengths as a function of $6/g^2$ for (a) scalar mesons, (b) vector mesons, and (c) baryons.

while the third quark can propagate backwards (the Appendix, subsection 4 and Ref. [10]).

In units of the temperature, the ρ and a_1 are already quite close to their $T\to\infty$ value of $6/g^2=5.55$. In contrast, the scalar channels are still visibly below this value even at $6/g^2=7.0$. (Of course on a $16^3\times 8$ lattice at $6/g^2=7.0$ we are measuring the screening propagators at a physical distance of a small fraction of a Fermi.) It should be noted that, if the transition is not first order, the fact that the pion mass vanishes in the chiral limit in the low-temperature phase, forces the π-σ multiplet to be strongly bound just above the transition where it becomes degenerate for $m_q=0$, since these masses must change continuously across the transition.

To further examine chiral symmetry restoration we follow the approach of Ref. [8], defining chiral meson propagators $M_S^{\pm}$, $M_{V0}^{\pm}$, and $M_{V1}^{\pm}$ (for definitions see the Appendix, subsection 4). A signature for chiral symmetry restoration is that in the chirally restored "phase" M_S^+/M_S^-, M_{V0}^+/M_{V0}^-, and M_{V1}^+/M_{V1}^- should vanish in the chiral limit ($m_q\to 0$) when the propagators are calculated using a source with definite chirality. Figure 10 shows these ratios as a function of $6/g^2$ and hence T. Note that the magnitude of M_{V0}^- is very small at even separations, making the ratio in Fig. 10(b) very large and noisy at these values of z for $6/g^2$ in the low-temperature phase, which is why these points do not appear in this figure. In the chiral limit, chiral symmetry restoration should force the nucleon propagator to vanish at even separations in the plasma phase. This trend is clear in Fig. 11. Taking

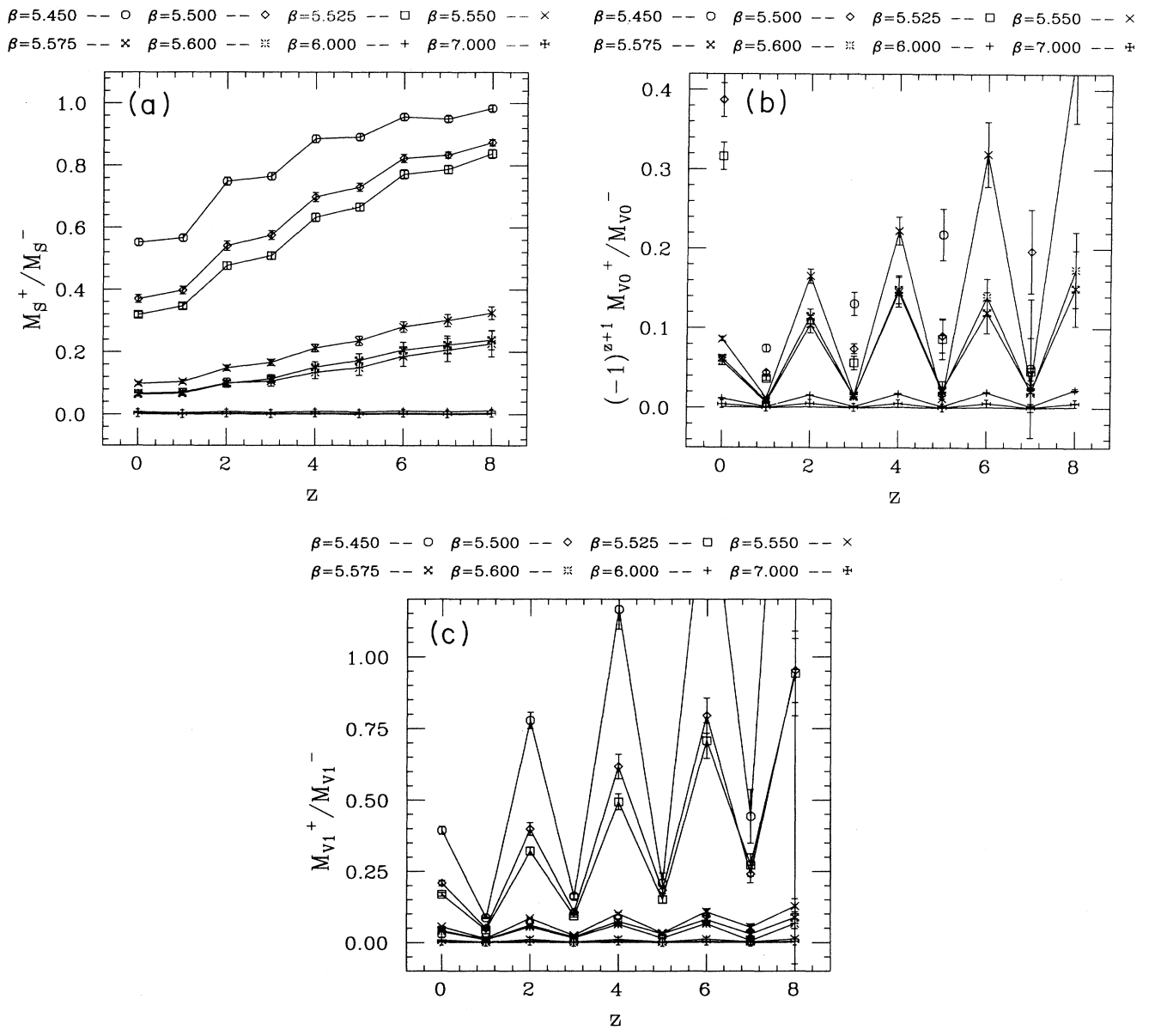

FIG. 10. Ratio of chiral meson propagators as a function of separation z for various $6/g^2$ values for (a) scalar mesons, (b) type-0 vector-meson propagators, and (c) type-1 vector-meson propagators.

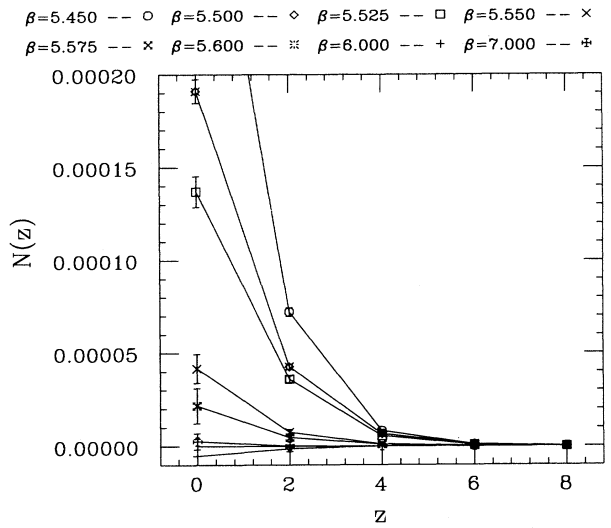

FIG. 11. Nucleon propagators as functions of z for z even and various $6/g^2$ values.

into account the fact that $m_q=0.0125\neq 0$, Figs. 10 and 11 show good evidence for chiral symmetry restoration for $T>T_c$.

Finally we note that the propagators for the ρ-b_1 and the a_1-ρ_2 systems in both polarizations are very similar to their free field counterparts by $6/g^2=7.0$ while those for the π-σ system are still quite different.

IV. CONCLUSIONS

In agreement with previous studies [3,25], the transition from nuclear matter to a quark-gluon plasma for two light quark flavors shows no evidence for being first order. However, the long relaxation times observed in Fig. 3 suggest that the system is close to a critical point. Thus our results are consistent with a second-order phase transition at $m_q=0$ and a rapid crossover with no phase transition where the quark masses are finite. The transition or crossover occurs at $6/g^2=5.54(2)$ corresponding to a temperature $T_c=155(9)$ MeV with a systematic uncertainty of $\sim 15\%$, consistent with previous estimates but far below the ~ 200 MeV found in the quenched theory. However, in at least one case we have observed apparent metastability over more than 1000 simulation time units.

The temporal Wilson-Polyakov line correlation functions indicate strong exponential screening of the interquark potential in the plasma phase. Perturbation theory indicates that the screening mass μ measured from these correlation functions is related to the Debye screening mass μ_D by $\mu=2\mu_D$ [27]. This yields a Debye screening length λ_D at the transition of $\lambda_D\sim 0.5$–0.8 fm. This result, to the extent that the relation between μ and μ_D is independent of perturbation theory, could be relevant to models for ψ/J suppression at high temperatures. In fact, simple potential models indicate that ψ/J formation should be suppressed for $\lambda_D \lesssim 0.4$ fm [31]. Taken at face value this would mean that we should expect to see ψ/J suppression only for $T\gtrsim 2T_c$. However, as the authors of [31] point out this ignores the temperature dependence of the coefficient of the Coulomb term in the heavy quark potential. Taking this into account will increase the critical value of λ_D and decrease the temperature for the onset of suppression. It is thus important to obtain more detailed predictions of the heavy quark potential in the quark-gluon plasma.

The hadron screening length measurements show clear evidence for chiral symmetry restoration in the plasma phase. The screening masses are consistent with a scenario in which the members of the π-σ chiral multiplet remain as bound states while the remaining states with hadronic quantum numbers that we have measured (ρ, a_1, b_1, N_1 and N') appear as unbound states of free quarks. However, measurements of the wave functions (more accurately, the analogue of the wave functions for propagation in a spatial direction) of these states show that they are local, with a characteristic size similar to the size of low-temperature hadrons [12]. Measurement of a finite string tension from spatial Wilson-Polyakov line correlation functions suggests that such states should indeed be bound. This suggests that a true understanding of the hadron screening lengths at high temperatures might emerge from studying the three-dimensional Yang-Mills-Higgs system which describes the high-temperature behavior of QCD.

We have seen good agreement of the topological susceptibilities with the prediction of the Ward identities, in the hadronic matter phase. Here, with only one mass, we were forced to use data from other work in order to extrapolate $\langle\bar{\psi}\psi\rangle$ to $m_q=0$. With the simulations at a lower quark mass, we will be able to make this extrapolation ourselves. In addition, we will be able to determine whether $\chi\propto m_q^2$ in the plasma phase, which would indicate that we really do have two light dynamical quark flavors.

When we have more realistic quark masses we will be able to measure the kaon screening lengths, which are also of some interest. We shall also measure the entropy density associated with a strange quark with a more physical mass, which should shed light on strangeness production in the quark-gluon plasma. We really need a lattice with a larger aspect ratio (N_s/N_t) to make the finite lattice size correction factors closer to one and thus reduce the systematic uncertainties involved in calculating entropy and energy densities and pressure. Such improved aspect ratios are also what is needed to more accurately extract the hadronic screening lengths. We need the zero-temperature values of the plaquette observable for the $6/g^2$ values of our simulations to enable us to extract partial pressures and energy densities, in order to determine the equations of state of hadronic matter. At $6/g_c^2$ we need to determine the zero-temperature hadron spectrum to enable a more accurate determination of T_c.

ACKNOWLEDGMENTS

The computations described in this paper were carried out on the connection machine CM2 at the Pittsburgh Supercomputer Center. We wish to thank the administration and staff of the Center for the extraordinary support they have given to this project. This work was sup-

ported by the U.S. Department of Energy under Contracts Nos. DE-FG02-85ER-40213, DE-AC02-86ER-40253, DE-AC02-84ER-40125, DE-FG02-91ER-40661, DE-FG05-85ER-250000, W-31-109-EN-38, and by the National Science Foundation under Grants Nos. NSF-PHY87-01775 and NSF-PHY91-16964.

APPENDIX: MEASURED QUANTITIES

1. Entropy

It would be extremely interesting to compare the equation-of-state of high-temperature QCD to phenomenological models, or perhaps someday even to experiment. In our simulations we have measured the raw quantities necessary to compute the energy and pressure. However, to compute the physical energy and pressure we must remove divergent and regularization dependent parts, which can be done by subtracting the energy and pressure measured at zero temperature. In the absence of the necessary zero-temperature simulations, we can use Euclidean invariance of the zero-temperature theory, which requires that at $T=0$ the energy and pressure be related by $\epsilon=-p$. This means that $(\epsilon+p)/T$, or the entropy density, can be computed without a zero-temperature subtraction.

Computing the energy and pressure requires knowing how the spatial and temporal lattice spacings depend on the coupling constants in the theory, where different couplings are used for the spatial and temporal directions. This dependence can be calculated in perturbation theory [32,21]. In principle, it is possible to use perturbation theory in this context since it is the coupling at the scale of the lattice spacing rather than the temperature which is relevant. However, the empirical β function determined by the dependence of $6/g^2$ at the thermal crossover on N_t differs from the perturbative β function by as much as a factor of 2 for lattice spacings in this range. Since, in the notation of Ref. [21], $c_\sigma+c_\tau=\beta$, where β is the β function, we can be assured that the perturbative corrections to the energy and pressure will suffer similar problems. In the formulas for the gluon and quark parts of the entropy density these perturbative corrections appear as multiplicative constants, so the reader can remove or rescale them as desired. The separation of the entropy into the gluon part of the fermion part is not really meaningful since the gluons and quarks are interacting; it simply reflects the way the entropy is computed.

We use the expressions:

$$s_g T=\frac{4}{3}\left[1-\frac{1.022}{6/g^2}\right]\frac{6}{g^2}(P_{\rm st}-P_{\rm ss})\ , \tag{A1}$$

$$s_{u,d}T=\left[1-\frac{1.279}{6/g^2}\right]\frac{n_f}{4}\left[\langle\bar\psi\not{D}_0\psi\rangle-\frac{1}{3}\sum_i\langle\bar\psi\not{D}_i\psi\rangle\right]\ . \tag{A2}$$

Here $P_{\rm st}$ and $R_{\rm ss}$ are the space-time and space-space plaquettes,

$$P_{\rm ss}=\langle{\rm Tr}(UUUU)\rangle_{\text{space-space plaquette}}\ , \tag{A3}$$

$$P_{\rm st}=\langle{\rm Tr}(UUUU)\rangle_{\text{space-time plaquette}}\ , \tag{A4}$$

and $\not{D}_\mu$ is the off-diagonal part of the fermion matrix in direction μ. Equations (A1) and (A2) are written in a form which emphasizes their vanishing at zero temperature. In evaluating the fermion entroy, we have used the identity

$$\left\langle\bar\psi\left[\not{D}_0+\sum_i\not{D}_i+m_q\right]\psi\right\rangle=\langle\bar\psi M\psi\rangle=3\ , \tag{A5}$$

where M is the complete fermion matrix and 3 is the number of color components, to write the quark entropy as

$$s_{u,d}T=\frac{4}{3}\left[1-\frac{1.279}{6/g^2}\right]\frac{n_f}{4}\left[\langle\bar\psi\not{D}_0\psi\rangle-\frac{3}{4}+\frac{1}{4}m_q\langle\bar\psi\psi\rangle\right]. \tag{A6}$$

2. Topological charge

Here we give a brief description of the cooling method for topological charge and susceptibility, referring the reader to the literature for more detailed discussions of the method and its justification. The cooling method for measuring topological charge on the lattice is based on the observation that the physical topological charge is associated with large scale structures. However, lattice gauge-field configurations also have contributions to their topological charge coming from distances on the order of the lattice spacing, which are artifacts of the lattice regularization and should be removed.

In the cooling method, one removes these lattice artifacts by locally smoothing the gauge fields by locally minimizing the plaquette action. This is done by updating each lattice gauge field using a Cabibbo-Marinari heat bath with $6/g^2=\infty$. If the lattice spacing is small enough and the lattice large enough, the topological charge rapidly approaches a plateau for which the ultraviolet contributions to the topological charge have been frozen out, and what remains is interpreted as the physical topological charge. Of course, if we continued this cooling long enough, the gauge configuration would eventually become trivial and the topological charge zero.

The lattice topological charge of the cooled configuration is then measured as

$$Q=\frac{1}{32\pi^2}\sum_{\rm sites}\epsilon_{\mu\nu\rho\sigma}\,{\rm Tr}(U_{\mu\nu}U_{\rho\sigma})\ , \tag{A7}$$

where $U_{\mu\nu}$ is the product of the SU(3) gauge-field matrices around a plaquette in the $\mu\nu$ plane. From Q one obtains the topological susceptibility

$$\chi=\frac{1}{V}\langle Q^2\rangle\ , \tag{A8}$$

where V is the space time volume of the lattice. In the chirally broken phase, the leading $O(m_q)$ contribution to χ is predicted to be

$$\chi=\frac{m_q}{n_f^2}\frac{n_f}{4}\langle\bar\psi\psi\rangle\ , \tag{A9}$$

where at infinite spatial volume we would evaluate $\langle\bar{\psi}\psi\rangle$ at $m_q=0$ to avoid having to define a subtraction scheme to remove its divergences for $m_q\neq 0$. In the chirally unbroken phase, $\langle\bar{\psi}\psi\rangle$ evaluated at $m_q=0$ vanishes, and χ is higher order in m_q. In fact, for small m_q we expect

$$\chi \propto m_q^{n_f} , \tag{A10}$$

where the constant of proportionality involves zero-temperature quantities not measured in these simulations.

Because a parallel implementation of the cooling method is less local than a serial implementation, there was a greater chance of changing the global topology during a cooling sweep than using a strictly local method. To check that this did not unduly bias the results, we also employed a method which cooled the lattice less rapidly at the beginning. This was achieved by using an underrelaxed version of the Cabibbo-Marinari heatbath method. This worked as follows. If the usual implementation of the Cabibbo-Marinari algorithm would require multiplying a particular SU(2) subgroup by the SU(2) matrix

$$V=\exp(i\alpha_\mu\sigma_\mu) \tag{A11}$$

we would instead multiply by

$$V_\lambda=\exp(i\lambda\alpha_\mu\sigma_\mu) , \tag{A12}$$

where $\lambda<1$ is the underrelaxation parameter. In Table IV, we list values for the topological susceptibility χ determined by the normal cooling method, using 25 cooling sweeps, and by first cooling the gauge fields slowly using the underrelaxed method with $\lambda=0.2$ for 25 sweeps, followed by 25 sweeps of normal cooling. The results of the two methods are clearly consistent.

3. Wilson-Polyakov line correlations

If $L(\mathbf{x})$ is the temporal Wilson-Polyakov line with spatial coordinates $\mathbf{x}$ on an $N_s^3\times N_t$ lattice then $T=1/aN_t$ is the temperature of the lattice and

$$\langle L(\mathbf{x})L^*(\mathbf{0})\rangle = A\exp[-V(r,T)/T] , \tag{A13}$$

where $r=|\mathbf{x}|$ and $V(r,T)$ is the potential between two heavy pointlike quarks. In the region where screening occurs, A is usually chosen to be $|\langle L\rangle|^2$ so that $V(\infty,T)=0$. Where screening occurs, we find that

$$|\langle L(\mathbf{x})L^*(\mathbf{0})\rangle-|\langle L\rangle|^2|\leq AF(r)\exp[-\mu(T)r] \tag{A14}$$

for r sufficiently large, where F is polynomial bounded and $\mu(T)$ is the screening mass. This implies that the potential is screened, viz.,

$$\frac{|V(r,T)|}{T}\leq F(r)\exp[-\mu(T)r] . \tag{A15}$$

Studies of these quantities in Ref. [27] have yielded estimates of $\mu(T)$ in the plasma phases of pure gauge theories.

We have adopted a slightly different approach based on a method which has proved effective in extracting the potential and string tension in zero-temperature lattice QCD. In this method the simple Wilson-Polyakov line is replaced by an extended "fuzzy" Wilson line constructed of "blocked" links, defined recursively by

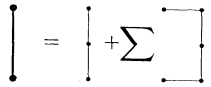

(A16)

where the sum is over the four "staples" in the x and y direction. This link matrix is then projected back into SU(3). Our blocked link at the Nth level of blocking thus has length 2^N. Our blocked temporal Wilson-Polyakov line is defined in terms of these blocked links just as our unblocked line was defined in terms of link fields. We then define a state of zero-momentum in the x-y-t hyperplane by summing over the x and y positions of the line. This fuzzy zero-momentum line we denote by $W(z)$, and define an unsubtracted correlation function

$$C(Z)=\frac{1}{V}\left\langle\sum_z W^*(z)W(z+Z)\right\rangle \tag{A17}$$

and a subtracted correlation function

$$P(Z)=\frac{1}{V}\left[\left\langle\sum_z W^*(z)W(z+Z)\right\rangle-N_s|\langle W\rangle|^2\right] . \tag{A18}$$

In the absence of screening $\langle W\rangle=0$ and $P(Z)=C(Z)$. Then for Z large enough

$$P(Z)=C(Z)\sim\exp[-V(N_t)Z] \tag{A19}$$

and if N_t is also large the potential $V(N_t)\simeq\kappa N_t$. The blocking is designed to make this asymptotic form a good approximation at relatively small Z.

When Debye screening occurs, $\langle W\rangle\neq 0$ and for large enough Z

$$P(Z)\sim\exp[-\mu(T)Z] , \tag{A20}$$

where again one expects blocking to enhance the approach to the asymptotic limit. $C(Z)$ now behaves as

$$C(Z)\sim\sum_{x,y}\exp[-V(x,y,Z,T)/T] , \tag{A21}$$

with V now the potential between smeared static sources, so that for Z sufficiently large

$$\frac{\sum_{x,y}V(x,y,Z,T)}{T}\sim\exp[-\mu(T)Z] \tag{A22}$$

and this potential is screened. If the screening is relatively weak, $C(Z)$ may be well approximated by an exponential in Z for intermediate Z, defining a potential linear in Z over this range, only becoming exponentially screened for large Z. For full QCD with dynamical quarks, where $\langle W\rangle\neq 0$ even in the hadronic matter phase, it is important to study both $C(Z)$ and $P(Z)$ to determine whether exponential behavior of the latter really represents screening or if it is just the reflection of the exponential behavior of $C(Z)$ indicative of a linearly rising potential.

To look for exponential behavior in our data, we have calculated effective masses by fitting each propagator locally to the form

$$C(Z)=A\{\exp(-\mu Z)+\exp[-\mu(N_s-Z)]\} \tag{A23}$$

and calculating the effective screening mass $\mu(Z)$ by solving

$$\frac{\exp[-M(Z-1)]+\exp[-M(N_s-Z+1)]}{\exp(-MZ)+\exp[-M(N_s-Z)]}=\frac{C(Z-1)}{C(Z)} \tag{A24}$$

for $M=\mu(Z)$. If $\mu(Z)\to\mu$ as $Z\to\infty$, μ is the desired screening length.

We have also considered spatial Wilson lines oriented in the x and y directions, with "fuzzy" or "blocked" forms created from blocked links defined by Eq. (A16), only now the staples are oriented in the y and t, respectively, x and t directions and having zero-momentum components in the x-y-t plane. Their correlations in the z direction are defined in the same way as those for the temporal lines. We have studied both the subtracted and unsubtracted forms of the propagator. Here, previous studies involving pure gauge theories without fermions have suggested that these correlations obey an area law defining a linear confining potential in both phases. For high temperatures, the behavior of such correlations is believed to be controlled by the three-dimensional Yang-Mills-Higgs system which QCD becomes when N_t is much smaller than any correlation lengths of the system. The area law behavior of these correlations is suggested to be due to the monopoles this theory allows [33].

4. Hadronic screening lengths

The hadron screening lengths have been obtained using a "corner" type wall source [6] on the $z=0$ hyperplane. On this hyperplane this source is $C\cos qt$ for x, y, and t all even and is zero otherwise. C is a constant, $q=\pi/N_4=\pi T$ is the lowest Matsubara frequency and the cos term incorporates the effects of the antiperiodicity in t. Since such a wall source is not gauge invariant we gauge fix to x-y-t Coulomb gauge to calculate our propagators. Following Ref. [7], we define the finite-temperature propagators for hadronic exitations obtained with local sinks by

$$\pi(z)=\sum_{x,y,t}|G(x,y,z,t)|^2 , \tag{A25a}$$

$$\rho_0(z)=\sum_{x,y,t}(-1)^t|G(x,y,z,t)|^2 , \tag{A25b}$$

$$\rho_1(z)=\sum_{x,y,t}[(-1)^x+(-1)^y]|G(x,y,z,t)|^2 , \tag{A25c}$$

$$a_{10}(z)=\sum_{x,y,t}(-1)^{x+y+z}|G(x,y,z,t)|^2 , \tag{A25d}$$

$$a_{11}(z)=\sum_{x,y,t}(-1)^{z+t}[(-1)^x+(-1)^y]|G(x,y,z,t)|^2 , \tag{A25e}$$

$$\sigma(z)=\sum_{x,y,t}(-1)^{x+y+z+t}|G(x,y,z,t)|^2 , \tag{A25f}$$

$$N(z)=\sum_{x,y,t}\cos qt\ \det G(x,y,z,t) , \tag{A25g}$$

where $G(x,y,z,t)$ is the quark Green's function for the above source. We fit our generic meson propagator $M(z)$ to the form

$$M(z)=A_+\{\exp(-m_+z)+\exp[-m_+(N_z-z)]\}+(-1)^zA_-\{\exp(-m_-z)+\exp[-m_-(N_z-z)]\} , \tag{A26}$$

where $A_\pm$ are coefficients, m_+ is the screening mass of the named meson, and m_- is the lightest opposite-parity meson coupling to the same source. The nucleon propagator is fit to the form

$$B(z)=A_+\{\exp(-m_+z)+(-1)^z\exp[-m_+(N_z-z)]\}+A_-\{(-1)^z\exp(-m_-z)+\exp[-m_-(N_z-z)]\} . \tag{A27}$$

Finally it is convenient to follow [8] and define chiral meson propagators, i.e., propagators for mesons which are eigenstates of the U(1)×U(1) chiral symmetry which remains exact on the staggered lattice. In terms of the above these are

$$M_S^\pm(z)=\pi(z)\pm\sigma(z) , \tag{A28a}$$

$$M_{V0}^\pm(z)=\rho_0(z)\pm a_{10}(z) , \tag{A28b}$$

$$M_{V1}^\pm(z)=\rho_1(z)\pm a_{11}(z) . \tag{A28c}$$

In the chiral symmetry restored "phase," in the chiral $m_q\to0$ all the M^+'s should vanish while the M^-'s remain finite.

[1] S. Gottlieb *et al.*, in *Lattice '91,* Proceedings of the International Symposium, Tsuhuba, Japan, 1991, edited by M. Fukugita *et al.* [Nucl. Phys. B (Proc. Suppl.) **26**, 308 (1992)].

[2] S. Duane and J. Kogut, Phys. Rev. Lett. **55**, 2774 (1985); S. Gottlieb, W. Liu, D. Toussaint, R. Renken, and R. Sugar, Phys. Rev. D **35** 2531 (1987).

[3] For a recent review see S. Gottlieb, in *Lattice '90,* Proceedings of the International Symposium, Tallahassee, Florida, 1990, edited by U. M. Heller, A. D. Kennedy, and S. Sanielevici [Nucl. Phys. B (Proc. Suppl.) **20**, 247 (1991)].

[4] R. Pisarski and F. Wilczek, Phys. Rev. D **29**, 338 (1984); F. Wilczek, J. Mod. Phys. A **7**, 3911 (1992).

[5] M. Teper, Phys. Lett. **162B**, 357 (1985); J. Hoek, M. Teper, and J. Waterhouse, Nucl. Phys. **B288**, 589 (1987).

[6] E. Marinari, in *Lattice '88,* Proceedings of the International Symposium, Batavia, Illinois, 1988, edited by A. S. Kronfeld and P. B. MacKenzie [Nucl. Phys. B (Proc. Suppl.) **9**, 209 (1989)].

[7] C. DeTar and J. Kogut, Phys. Rev. Lett. **59**, 399 (1987); Phys. Rev. D **36**, 2828 (1987).

[8] S. Gottlieb, W. Liu, R. L. Renken, R. L. Sugar, and D. Toussaint, Phys. Rev. Lett. **59**, 1881 (1987).

[9] A. Gocksch, P. Rossi, and U. M. Heller, Phys. Lett. B **205**, 334 (1988); A. Ukawa, in *Lattice '88* [6], p. 463; K. Bitar *et al.*, Phys. Rev. D **43**, 2396 (1991).

[10] A. Irbäck, in *Lattice '90* [3], p. 280; K. D. Born *et al.*, Phys. Rev. Lett. **67**, 302 (1991).
[11] A. Gocksch, Phys. Rev. Lett. **67**, 1701 (1991).
[12] C. Bernard, M. C. Ogilvie, T. DeGrand, C. DeTar, S. Gottlieb, A. Krasnitz, R. L. Sugar, and D. Toussaint, Phys. Rev. Lett. **68**, 2125 (1992).
[13] M. Teper, Phys. Lett. B **183**, 345 (1987).
[14] W. Liu, in *Lattice '90* [3], p. 149.
[15] The HEMCGC Collaboration, K. M. Bitar *et al.*, Phys. Rev. Lett. **65**, 2106 (1990); Phys. Rev. D **42**, 3794 (1990).
[16] S. Gottlieb, W. Liu, R. L. Renken, R. L. Sugar, and D. Toussaint, Phys. Rev. Lett. **59**, 1513 (1987).
[17] F. R. Brown *et al.*, Phys. Rev. Lett. **67**, 1062 (1991); K. M. Bitar *et al.*, in *Lattice '91* [1], p. 259; (unpublished).
[18] C. Bernard, M. C. Ogilvie, T. DeGrand, C. DeTar, S. Gottlieb, A. Krasnitz, R. L. Sugar, and D. Toussaint, Phys. Rev. D **45**, 3854 (1992).
[19] A. D. Kennedy, J. Kuti, S. Meyer, and B. J. Pendleton, Phys. Rev. Lett. **54**, 87 (1985); S. A. Gottlieb, J. Kuti, D. Toussaint, A. D. Kennedy, S. Meyer, B. J. Pendleton, and R. L. Sugar, *ibid.* **55**, 1958 (1985).
[20] P. Bacilieri *et al.*, Nucl. Phys. **B343**, 228 (1990); S. Cabasino *et al.*, in *Lattice '90* [3], p. 399; R. Gupta *et al.*, Phys. Rev. Lett. **43**, 2003 (1991); K. M. Bitar *et al.* in *Lattice '90* [3], p. 362.
[21] F. Karsch and I. O. Stamatescu, Phys. Lett. B **227**, 153 (1989).
[22] R. V. Gavai *et al.*, Phys. Lett. B **241**, 567 (1990).
[23] J. Engels, F. Karsch, and H. Satz, Nucl. Phys. **B205**, 239 (1982).
[24] F. C. Hansen and H. Leutwyler, Nucl. Phys. **B350**, 201 (1991).
[25] S. Gottlieb, W. Liu, R. L. Renken, R. L. Sugar, and D. Toussaint, Phys. Rev. D **41**, 622 (1990).
[26] K. M. Bitar *et al.*, Phys. Rev. D **44**, 2090 (1991).
[27] N. Attig *et al.*, Phys. Lett. B **209**, 65 (1988); A. Irbäck *et al.*, Nucl. Phys. **B363**, 34 (1991).
[28] F. Karsch and H. W. Wyld, Phys. Lett. B **213**, 505 (1988).
[29] E. Manousakis and J. Polonyi, Phys. Rev. Lett. **58**, 847 (1987).
[30] C. Bernard, T. A. DeGrand, C. DeTar, S. Gottlieb, A. Krasnitz, M. C. Ogilvie, R. L. Sugar, and D. Toussaint, in *Workshop on Fermion Algorithms,* edited by H. J. Hermann and F. Karsch (World Scientific, Singapore, 1991); in *Lattice '91* [1], p. 262; (unpublished).
[31] F. Karsch, M. T. Mehr, and H. Satz, Z. Phys. C **37**, 617 (1988); T. Matsui and H. Satz, Phys. Lett. B **178**, 416 (1986).
[32] F. Karsch, Nucl. Phys. **B205**, 285 (1982).
[33] F. Brandstaeter, G. Schierholz, and U.-J. Wiese, Phys. Lett. B **272**, 319 (1991).